Automating Building Damage Reconnaissance to Optimize Drone Mission Planning for Disaster Response

Da Hu[1], A.M.ASCE, Shuai Li[2,*], Ph.D., A.M.ASCE, Jing Du[3], Ph.D., M.ASCE, and Jiannan Cai[4], Ph.D., A.M.ASCE

[1] Department of Civil and Environmental Engineering, The University of Tennessee, 851 Neyland Drive, Knoxville, TN 37996; Department of Civil and Environmental Engineering, Kennesaw State University, 1100 South Marietta Pkwy, Marietta, GA 30060; email: dhu3@kennesaw.edu

[2] Department of Civil and Environmental Engineering, The University of Tennessee, 851 Neyland Drive, Knoxville, TN 37996; email: sli48@utk.edu

[3] Engineering School of Sustainable Infrastructure & Environment, University of Florida, 1949 Stadium Road 454A Weil Hall, Gainesville, FL 32611; email: eric.du@essie.ufl.edu

[4] School of Civil and Environmental Engineering, and Construction Management, The University of Texas at San Antonio, 501 W César E Chávez Blvd, San Antonio, TX 78207; email: jiannan.cai@utsa.edu

* Corresponding Author, Shuai Li, email: sli48@utk.edu

ABSTRACT

Rapid reconnaissance of building damage is critical for disaster response and recovery. Drones have been utilized to collect aerial images of affected areas in order to assess building damage. However, there are two challenges. First, processing many aerial images to detect and classify building damage based on a consistent standard remains laborious and complex, necessitating a new automated solution to achieve accurate building damage detection and classification. Second, drone operations during disaster response rely primarily on human operators' experience and seldom use the obtained building damage information to optimize drone mission planning. Therefore, this study proposes a new method, which automates building damage reconnaissance with drone mission planning for disaster response operations. Specifically,

a deep learning method is developed to detect and classify building damages using a newly labeled dataset consisting of 24,496 distinct instances of building damage. This deep learning method is validated, achieving 71.9% mean average precision. In addition, building damage information is modeled and integrated into mission planning, in order to optimize drones' task assignments and route calculations. A tornado disaster in Tennessee is used as a case study, to quantitatively evaluate this methodology. The present study concludes that optimal drone mission planning during disaster response can be augmented using accurate building damage information acquired from deep learning methods.

INTRODUCTION

Natural disasters, such as earthquakes and tornadoes, lead to massive building damage, resulting in deaths, injuries, and destruction of property. According to the National Oceanic and Atmospheric Administration (NOAA), more than 20 climate-related disasters occurred in 2021 across the US (Doyle Rice 2022), claiming at least 688 deaths and leading to over $145 billion in economic losses. After the disasters, rapid and accurate assessment of building damages is crucial for both immediate and long-term urban disaster responses. First, assessing building damages provides essential information that enables first responders to prioritize search and rescue (SAR) operations and efforts to save trapped victims, protect properties, and perform emergency response logistics. First responders are the main force to respond to these disasters and to conduct SAR operations. Disasters such as earthquakes, floods, and tornadoes often lead to traffic "paralysis," which can prevent first responders from entering damaged areas and may delay SAR operations (Chang et al. 2012), imposing significant challenges to ensuring safe and efficient SAR. Acquiring accurate damage information on the affected areas could save enormous amounts of time as first responders plan response efforts. In addition, most casualties from major disasters are associated with structural collapses (Geiß et al. 2014). For example, the extent of damage to buildings is an important indicator of an earthquake's magnitude, which in turn provides a measure of the scale of human and property losses in that area (Lei et al. 2010). Having accurate information regarding building damages, therefore, could help first responders in prioritizing their SAR operations. Second, acquiring information on building damages at a large scale could help the community better plan for future disaster preparation, response, and mitigation.

The information can also be utilized to improve the design of insurance programs. Despite the importance of acquiring accurate and timely building damage information for effective and efficient disaster response, mitigation, and recovery, the current manual and outmoded manual practices are unable to provide this.

This study develops a new method for drone-based disaster reconnaissance to map the building damages in affected areas. Drones hold great potential for emergency reconnaissance, because they can deploy quickly, collect heterogeneous sensing data, survey areas humans cannot reach, and can identify areas with the most severe damage. There has been growing use of drones in disaster response, particularly in damage assessment, but there are two knowledge gaps that must be closed for the optimal deployment of this solution. First, the information retrieval from drone-based images and videos is superficial, providing limited information for practical applications. Although solutions based on deep learning have been developed to accelerate visually-based damage assessment, levels of building damage have seldom been accurately classified. Damage levels are usually categorized based on criteria from the Federal Emergency Management Agency (FEMA) and the National Weather Service (NWS), and accurately distinguishing the levels of tornado-induced building damage in drone-acquired aerial images is beyond the capabilities of existing methods. Second, utilizing drones for surveying disaster areas is a dynamic and evolving task, and the dynamic information obtained by drones should be actively exploited for drone mission planning. This is critical for disaster response, given the time constraints and the limited availability of resources. Current practices on drone mission planning in disaster areas focus mainly on area coverage; they are not geared toward integrating acquired damage information to optimize drone task assignments or route generation. Integrating drone-acquired information from initial surveys could also improve the planning of various subsequent drone-based tasks and missions, such as detailed assessment and package delivery.

To address these technical challenges, this research proposes a deep-learning-based method for detecting and classifying different levels of building damage and then incorporating that information for drone mission planning, so as to optimize task assignments for disaster reconnaissance and response. The contribution of this study is two-fold. First, a new deep learning method based on YOLO5 is proposed to endow the drone with the intelligence to detect and classify seven distinct categories of building damage, thus providing refined classification information for disaster response. In addition, this research has led to a newly labeled dataset consisting of 24,496 instances of building damage after tornadoes, based on the Enhanced Fujita (EF) scale, which provides an essential basis for advancing deep learning methods for automated building damage reconnaissance after disasters. Second, the detected and classified building damages are exploited in an optimization model for drone mission planning during disaster response, considering the physical and resource constraints. By integrating building damage information into the mission planning model, the drone task assignments and route generations can be optimized, thereby further augmenting the disaster response protocol. The developed methods are validated and evaluated using real data from a tornado disaster in Tennessee, which further consolidates the potential of the proposed methods.

LITERATURE REVIEW

Related studies on building damage assessment

Damage assessment of structures, including buildings and bridges, under natural disasters has been widely studied in the structural engineering and natural hazard engineering communities. Originally developed by the Pacific Earthquake Engineering Research Center, the performance-based earthquake engineering framework (Cornell et al. 2002) is a generally accepted and adopted risk quantification method for earthquake hazards (Baker and Cornell 2008; Du et al. 2020; Du and Padgett 2021), and has had its applications extended to other disasters such as hurricanes and tornadoes (Herbin and Barbato 2012; Roueche et al. 2017). Within this framework, one critical component is fragility modeling, which delivers a conditional probability estimate of the exceedance of a certain structural damage state and establishes the connection between natural hazard intensities and structural damage potential (Du et al. 2021). In earthquake engineering, various methods have been developed for modeling fragility functions based on analytical models (Du et al. 2021; Du and Padgett 2020; Nielson and DesRoches 2007; Padgett and DesRoches 2008), post-hazard reconnaissance (Buratti et al. 2017; Giordano et al. 2021), and expert judgment (FEMA 2012). For wind-related hazards, the Florida Public Hurricane Loss Model (Chen et al. 2009; Pinelli et al. 2011) and HAZUS-MH (Vickery et al. 2009) are commonly used to estimate building damage. Despite the wide applications in performance-based building design, pre-disaster planning, and post-disaster response and recovery, fragility models still admit of substantial uncertainties and are more suitable for rapid regional-level post-hazard damage screening.

When it comes to assessing damages done to individual structures, the post-disaster evaluation of existing buildings relies largely on professionals' field surveys and visual observations (Xie et al. 2016; Yamazaki et al. 2005), which are time-consuming, labor-intensive, and vulnerable to subjective judgments. To address this limitation, data-driven methods have been developed to automatically analyze images from disaster sites for building damage assessment. Some methods (see, e.g., Cooner et al. (2016)) leverage traditional machine learning algorithms (e.g., random forest) to assess post-earthquake structural damage from handcrafted image features, where the performance depends heavily on feature selections. Schaefer et al. (2020) developed an automatic workflow which generates a 3D dense point cloud from images collected by a drone; the disaster damage is then quantified by comparing pre-hurricane and post-hurricane point clouds. Zhang et al. (2020) developed a remote sensing information-extraction method which uses thermal and RGB images to recognize structural damage to infrastructures caused by earthquakes. This method uses spectrum, shape, texture, space, and other characteristics of buildings to segment building damages in a 3D building model. However, these methods require extensive computational power to generate 3D models and identify damages, which is not feasible for online damage detection at disaster sites.

More recently, deep learning methods have been widely used in computer vision tasks and have been demonstrated to be effective in a variety of fields, including material recognition (Chen et al. 2021; Hu and Li 2022), synthetic image augmentation (Chen et al. 2022), and affordance segmentation (Hu et al. 2020). For the task of building damage detection, Miura et al. (2020) developed a convolutional neural network (CNN)-based approach for estimating building damage based on post-disaster aerial images, where the level of building damage is divided into non-collapsed, blue-tarp-covered, and collapsed categories. This CNN method achieved high accuracy on the aerial image data collected after the 2019 Chiba typhoon. Zhu et al. (2021) developed a novel CNN-based model for building damage segmentation based on Mask R-CNN architecture, by exploring hierarchical spatial relationships among different objects. Their method was validated using the Instance Segmentation in Building Damage Assessment (ISBDA) dataset, where building damages were classified as slight, severe, or debris-level.

Despite these achievements, there remain two limitations. First, the performance of deep-learning-based building damage detection is largely influenced by the quality and generalizability of training data. While there are several aerial image datasets (Pi et al. 2020; Rahnemoonfar et al. 2021; Zhu et al. 2021) which can be used for disaster assessment, very few of them focus on tornado disasters, thus limiting the application in post-tornado reconnaissance. Moreover, in most existing studies, building damages are simply classified into three coarse levels, which contrast with typical damage assessment tools (e.g., HAZUS for earthquakes, hurricanes, etc., and the EF scale for tornadoes) and hamper the integration of estimated building damages with downstream structural analyses. To overcome this limitation, this study introduces a new dataset for damaged buildings after major tornadoes across 25 different cities in the US and Canada, where building damage is classified into seven classes based on EF scale. Second, the deep learning methods developed in most studies have complex architectures and cannot achieve satisfactory accuracy. In this study, a new, lightweight deep learning network is designed by integrating spatial and channel attention mechanisms into YOLOv5 architecture, so as to ensure both accuracy and computational efficiency.

Related studies on drone mission planning

Equipped with different sensors, such as cameras, LiDAR, GPS, and IMU, drones can be powerful tools for disaster response; they have been deployed in real-world scenarios, including hurricane Katrina (Murphy et al. 2008), the 2013 Moore-Newcastle tornado (Grogan et al. 2021), and the 2013 Lushan earthquake (Qi et al. 2016). Studies have also been dedicated to developing methods for various drone-assisted tasks, such as SAR (Chen et al. 2020; Hu et al. 2019, 2022a; b) and structural damage assessment (Kakooei and Baleghi 2017; Schaefer et al. 2020).

Drone mission planning is a critical component for ensuring the efficiency of disaster reconnaissance and response. Various mission planning strategies have been devised as optimization problems, i.e., to maximize area coverage for drone surveys considering diverse constraints, such as power, maneuverability, distance, and data transmission quality (Gramajo and Shankar 2017; Huang et al. 2020; Li et al. 2018; Yu et al. 2020). Some research, e.g., by Nedjati et al. (2016) and Hayat et al. (2020), has focused on multi-drone path-planning for optimal area coverage. In addition, Xu et al. (2021) have formulated drone path planning as a constrained multi-objective optimization problem accounting both for navigation and imaging performance, which is solved using a heuristic search method. Van Huynh et al. (2022) have proposed an optimal drone path-planning approach to minimize drones' mission completion time and energy consumption. Their approach investigated peer-to-peer drone-IoT sensing and clustering drone-IoT sensing networks for the optimization of energy consumption.

Despite drones' great potential for disaster response, almost all existing studies have focused primarily on optimizing area coverage for drone surveys, while neglecting the importance of mission-specific priorities. In building damage reconnaissance, it is critical for drones to be able—despite limited resources, (e.g., battery life, number of drones)—to rapidly acquire large-scale information about building damages, for further structural analyses, risk assessment, and disaster response and mitigation. To ensure the efficiency of building damage reconnaissance, this study proposes a new drone-mission-planning mechanism which maximizes total surveyed degree of damage via a team-orienteering problem that accounts for operational constraints.

METHODOLOGY

Fig. 1 shows the overall research framework, which consists of three steps. In the first, aerial video data in the aftermath of significant tornadoes is collected from online websites and recorded by the authors. Image frames are extracted from the video, and buildings with damage are annotated using bounding boxes within the images. In the second step, a deep learning network is designed to detect and classify building damage from aerial images. The annotated image dataset is used to train the network, and performance is evaluated. The generalizability of the model is also investigated, by testing the network at new disaster sites. In the third step, the detected building damage is used to create a digital building damage map. Drone mission-planning is treated and solved as an optimization problem, construed specifically as a team-orienteering problem (TOP). The objective is to maximize the total surveyed degree of damage (DOD), given operational constraints, such as drone battery life and the number of drones. The total surveyed DOD is the sum of the DOD for each building. Several optimization methods are investigated, and their performance under various scenarios is evaluated. The technical details of the proposed framework are explicated below.

EFSBD dataset

Data collection

In this study, a total of 34 aerial videos were collected in the aftermath of tornadoes. Of these, 32 were obtained from online websites using a query of keywords (e.g., ‘tornado’, ‘drone’, ‘UAV’), and two videos were recorded by the authors in the aftermath of the 2020 Nashville tornado. In addition, 33 of these videos were collected in the US and one in Barrie, ON, Canada. Fig. 2 displays selected US tornadoes represented in the dataset and their associated intensities and approximate locations. The intensity of these tornadoes varies from EF2 to EF4. The tornadoes hit 25 different cities, and significant residential damages were reported in each case.

Data annotation

The video data was first converted to individual frames. One frame was then extracted from at least 30 consecutive frames to achieve a more visually heterogeneous dataset. Note that blurry images were omitted, as were those that do not depict damaged buildings. In total, 3,045 aerial images were collected in the dataset. The level of building damage is annotated based on the EF Scale, which is used to rate the intensity of a tornado based primarily on structural damage and wind speed (Doswell et al. 2009). The EF scale has also been adopted as the standard method for rating building damages caused by tornadoes. Table 1 presents each damage level with damage indicators. The EF scale defines six levels of building damage: minor, moderate, considerable, severe, devastating, and incredible. The level of damage is determined based on damage indicators in accordance with those developed by the National Wind Science and Engineering Center (McDonald et al. 2009). Note that a building with a roof covered by roofing tarps is defined as an additional level of damage. This is because it is difficult to determine the exact damage level for a building covered by roofing tarps from aerial images. Fig. 3 presents examples of buildings with different levels of damage.

Image annotation was conducted using the RectLabel tool, by drawing bounding boxes for damaged buildings appearing in each image. The annotators were trained to get familiar with the building damage assessment criteria for tornadoes as shown in Table 1. The images were then annotated in accord with these criteria. The annotated dataset is named the Enhanced Fujita Scale Building Damage (EFSBD). Fig. 4 shows the statistics of the EFSBD dataset. The dataset consists of a total of 24,496 instances of buildings with annotated damages. Specifically, the dataset has 4,997 buildings with minor labels, 7,223 buildings with moderate damage, 5,540 buildings with considerable damage, 2,419 buildings with severe damage, 832 buildings with devastating damage, 526 buildings with incredible damage, and 2,959 buildings covered by roofing tarps.

Data uniqueness

The EFSBD provides several unique features, compared to existing natural disaster datasets for damage assessment (see Table 2).

- First, while there are several aerial image datasets for disaster assessment, very few datasets are mainly focused on tornado disasters. Among the datasets given in Table 2, ISBDA (Zhu et al. 2021) is the only image dataset that consists of tornado scenes. However, in ISBDA, the number of images collected from tornado disasters is very limited. The number of annotated building instances is also relatively small. Furthermore, ISBDA follows the "Joint Damage Scale" proposed by Gupta et al. (2019), which was developed for satellite images with low resolution. As such, this scale may not be suitable for assessing building damages based on drone images.
- Second, EFSBD was developed based on the EF scale, which is used as a guideline by the NWS tornado disaster survey team. Moreover, a building covered with roofing tarp is classified as a separate category, due to the difficulties in recognizing its exact level of damage. In other existing datasets, roofing tarp is either incorporated into other categories (as per, e.g., RescueNet) or ignored (as per, e.g., Volan2018 and ISBDA).
- Third, the EFSBD consists of a total of 24,496 instances of damaged buildings, which is much higher than ISBDA, FloodNet, and RescueNet. Volan2018 has more building instances, but it

extracts 30 FPS, resulting in large overlaps between image frames. Hence, many building instances in Volan2018 may originate from the same building in neighboring frames. For example, Volan2018 collected 5,949 building instances from an 84-second video clip. This could lead to poor generalizability of the trained model to new disaster sites.

Building damage recognition

This section elaborates on the network for building damage detection at disaster sites. Our study adopts You Only Look Once (YOLO) architecture, which is a fast multi-object detection algorithm (Redmon et al. 2016). Object detection in YOLO is done as a regression problem to estimate bounding box coordinates and class probabilities. CNN is employed to detect objects with a single forward propagation through the network, which can be trained in an end-to-end manner. The proposed deep learning method is adapted from the YOLOv5 network. YOLOv5 is the latest upgrade from YOLOv3, with significant modifications, such as the addition of mosaic augmentation and customizing backbone network with Cross Stage Partial Network (CSPNet) and Spatial Pyramid Pooling – Fast (SPPF) (Jocher et al. 2021). YOLOv5 architecture is divided into YOLOv5s (small), 5m (medium), 5l (large), and 5x (extra-large), depending on the number of learnable parameters in the network. The number of learnable parameters, in turn, is controlled by two parameters: depth multiple and width multiple. YOLOv5s is the smallest model among the four variants, with a depth multiple of 0.5 and a width multiple of 0.33. Typically, the predictive power of the family YOLOv5 models improves with increases in the size of the network.

In this study, YOLOv5s architecture is selected to ensure the inference speed of the network. The fast inference speed has at least two advantages for disaster response. First, computational cost is a major constraint on the timely retrieval of building damage information from aerial images. A small network can be deployed into an embedded planform, thus enabling the detection to run on drones. Second, the network can provide disaster surveyors with timely disaster information via live stream with predicted damages. This is important, as it allows surveyors to better understand the scale of disaster damage in the field. The YOLOv5s consists of three components: backbone network, detection neck, as well as three detection heads. The architecture is detailed as follows.

The input images are first preprocessed using the mosaic method, which is a data augmentation method which improves network performance on small objects. The backbone network is used to extract features at various levels from images; it is built based on CSPNet (Wang et al. 2020). The CSPNet integrates the gradient changes into the feature map from beginning to end. As such, the CSPNet can reduce the computation cost while maintaining the inference power of the network. Each CSPNet network consists of three convolutional layers cascaded by various bottlenecks. SPPF is included as the last-layer backbone, aiming to extract fine and coarse information by simultaneously pooling from multiple kernel sizes (5, 9, 13). The detection neck is built based on the Path Aggregation Network (PANet) (Liu et al. 2018) and serves to boost information flow at different levels. PANet is an improvement of the Feature Pyramid Network (FPN) with an additional bottom-up pathway. The detection neck aims to get feature pyramids, each of which is used to identify objects in various sizes and scales. The detection neck consists of four CSPNet blocks. The three feature maps with different scales are used to predict targets of various sizes. Finally, these feature maps are divided into grids, and each grid consists of multiple anchors for predicting the bounding box for the object. Fig. 5 presents an overview of the improved YOLOv5s architecture. Two improvements were introduced: the addition of an attention mechanism and the replacement of bounding box regression loss.

Adding the attention mechanism. The attention mechanism was developed by studying humans' cognitive processes in visual perception. Specifically, humans selectively focus on particular regions of the scene while ignoring other regions (always known as backgrounds). For example, humans learn to concentrate on useful objects that appear in a scene during an image-classification task. This mechanism enables humans to quickly perceive and understand the visual context. The attention mechanism has been widely used in computer vision and has been shown to be effective (Guo et al. 2022). For CNN, every channel of a feature map may be representative of a different object (Chen et al. 2017). Based on this characteristic, a channel attention mechanism was proposed to capture channel-wise relationships, thereby improving the representational ability of the network. The Squeeze-and-Excitation Network (SENet) (Hu et al. 2017) is the pioneering work for channel-attention modeling; it recalibrates weight for the feature map channels. The main drawback of SENet is that it ignores positional information. Coordinate attention (Hou et al. 2021) was developed to address this limitation, by embedding positional information into channel attention. In this study, a coordinate attention mechanism is added to the detection neck, as shown in Fig. 5. This attention module is lightweight and enables the YOLOv5s network to focus on important regions at the expense of a little computational cost.

Fig. 6 shows the schematic flowchart of the coordinate attention module, which consists of two steps. First, two spatial extents of pooling kernels are used to encode each channel of the feature map along the horizontal and vertical directions, respectively. The output is a pair of direction-aware feature maps. Eq. (1) and Eq. (2) give the respective definitions of the two pooling operations, where $\mathbf{X}$ is the input feature map, and $\mathrm{GAP}^{\mathrm{h}}$ and $\mathrm{GAP}^{\mathrm{w}}$ represent vertical and horizontal directions, respectively.

$$\mathbf{z}^h = \mathrm{GAP}^h(\mathbf{X}) \tag{1}$$

$$\mathbf{z}^w = \mathrm{GAP}^w(\mathbf{X}) \tag{2}$$

In the second step, direction-aware feature maps are first concatenated, followed by a 1 x 1 convolutional operation. The output from the convolutional operation is split into two separate tensors along the spatial dimension. Then, two convolutional operations, each with kernel size 1 x 1, are applied to the two tensors, respectively. This process is represented by Eqs. (3) – (7), where δ is a non-linear activation operation, σ is the sigmoid function, F_1 represents the 1 x 1 convolutional operation, and F_{h} and F_{w} represent convolutional transformations on $\mathbf{f}^h$ and $\mathbf{f}^w$, respectively.

$$\mathbf{f} = \delta\left(F_1\left([\mathbf{z}^h, \mathbf{z}^w]\right)\right) \tag{3}$$

$$\mathbf{f}^h, \mathbf{f}^w = \mathrm{split}(\mathbf{f}) \tag{4}$$

$$\mathbf{g}^h = \sigma\left(F_h\left(\mathbf{f}^h\right)\right) \tag{5}$$

$$\mathbf{g}^w = \sigma\left(F_w(\mathbf{f}^w)\right) \tag{6}$$

$$\mathbf{Y} = \mathbf{X}\mathbf{g}^h\mathbf{g}^w \tag{7}$$

Replacing bounding box regression loss. The default bounding box regression loss function used to train YOLOv5 is Complete-IoU (CIoU), which was developed based on Distance-IoU (DIoU) by imposing the consistency of aspect ratio. In this study, CIoU is replaced by alpha-IoU loss (He et al. 2021) to train the network. The alpha-IoU is a family of power IoU losses designed for bounding box regression; it has been demonstrated to be effective in small datasets and noisy bounding boxes. The alpha-IoU is defined in Eq. (8), where $\boldsymbol{b}$ and $\boldsymbol{b}^{gt}$ denote the central points of predicted bounding box B and ground-truth bounding box B^{gt}, respectively, ρ is the Euclidean distance, c is the diagonal length of the smallest enclosing box, β is a positive trade-off parameter, v is used to measure the consistency of aspect ratio, and α is the modulating parameters. When α is equal to 1, $L_{\alpha\text{-CIoU}}$ becomes CIoU loss function. When $\alpha > 1$, $L_{\alpha\text{-CIoU}}$ has more emphasis on high-IoU objects and learns faster on these objects. In this study, α is set to 3 in order to increase the loss and gradient on high-IoU objects for accurate object localization.

$$L_{\alpha-\mathrm{CIoU}} = 1 - \mathrm{IoU}^{\alpha} + \frac{\rho^{2\alpha}(\boldsymbol{b},\boldsymbol{b}^{gt})}{c^{2\alpha}} + (\beta v)^{\alpha} \tag{8}$$

Drone mission planning

Drones can quickly survey large disaster areas and collect disaster information to provide rapid post-disaster damage estimates. In this study, the drone survey is divided into three steps. In the first step, the drone is deployed to disaster sites and collects video data for subsequent damage assessments. In the second step, the proposed building damage detection method is used to recognize damaged buildings from the collected videos. The recognition results can be used to generate a building damage map of the area. Finally, the second stage of damage mapping is conducted to generate details of assessment for each building, such as high-resolution images and 3D models. This section elaborates on the drone mission planning of the second stage.

Problem formulation

Drone mission planning is formulated as a TOP (Chao et al. 1996). In the TOP, a total of n damaged buildings i is given, each with a damage index r_i. The distance d_{ij} from building i to building j is calculated using Euclidean distance. The flight speed of drone k is s_k. Considering the operational constraints (e.g., battery life and flight speed) of drones, not all damaged buildings can be surveyed from a single mission. The battery capacity is directly associated with the flight duration T_{max} of the drone. The objective of the

TOP is to identify the route which maximizes total surveyed DOD given the operational constraints. Each of the buildings can be visited at most once.

Let G = {**V**, **E**} be a graph. **V**\{0} = {*1*, …, *n*} denotes the vertices of the graph, which represent damaged buildings. Each pair of vertices $i \in \mathbf{V}$ and $j \in \mathbf{V}$ forms an edge $\{i, j\} \in \mathbf{E}$. **K** = {1, …, m} represents a set of m drones. Let the building damage indices be $r_i > 0$ (with $r_0 = 0$). t_i is the time required to survey building $i \in \mathbf{V}$. Let binary variable x_{ijk} be equal to 1 if path $(i, j) \in \mathbf{E}$ is traversed by drone k, and 0 otherwise. Let y_{ik} equal 1 if $i \in \mathbf{V}$ is visited by the drone k, and 0 otherwise. The mathematical formulation for the TOP can be represented by Eqs. (9) – (17).

$$\text{maximize } \sum_{i\in\mathbf{V}} r_i \sum_{k\in\mathbf{K}} y_{ik} \tag{9}$$

subject to

$$\sum_{j\in\mathbf{V}} x_{ijk} = y_{ik} \quad \forall i \in \mathbf{V}, k \in \mathbf{K} \tag{10}$$

$$\sum_{j\in\mathbf{V}} x_{jik} = y_{ik} \quad \forall i \in \mathbf{V}, k \in \mathbf{K} \tag{11}$$

$$\sum_{k\in\mathbf{K}} y_{0k} \le m \tag{12}$$

$$\sum_{k\in\mathbf{K}} y_{ik} \le 1 \qquad i \in \mathbf{V}\backslash\{0\} \tag{13}$$

$$\sum_{(i,j)\in\delta^{+}(\mathbf{S})} x_{ijk} \ge y_{bk} \qquad \forall S \subseteq \mathbf{V}\backslash\{0\}, b \in \mathbf{S}, k \in \mathbf{K} \tag{14}$$

$$\sum_{(i,j)\in\mathbf{E}} \frac{d_{ij}}{s_k} x_{ijk} + t_i y_{ik} \le T_{max} \qquad \forall k \in \mathbf{K} \tag{15}$$

$$y_{ik} \in \{0,1\} \qquad \forall i \in \mathbf{V}, k \in \mathbf{K} \tag{16}$$

$$x_{ijk} \in \{0,1\} \qquad \forall (i,j) \in \mathbf{E}, k \in \mathbf{K} \tag{17}$$

Eq. (9) is the objective function used to maximize the total surveyed DOD. Eqs. (10) – (17) are constraints for the optimization problem. Specifically, constraints (10) and (11) are assignment constraints which ensure that one edge enters and one edge leaves each visited vertex. Constraint (12) ensures that the deployed drone does not exceed the number of drones. Constraint (13) ensures that every building is surveyed at most once. Constraint (14) imposes that each route is connected. Constraint (15) is the time constraint. Constraints (16) and (17) are variable definitions.

Mission planning solver

The TOP is known as an NP-hard problem. Significant research efforts have been dedicated to solving the TOP, and many heuristic-based algorithms have been developed. Selecting the appropriate algorithm is critical for ensuring that time-sensitive disaster damage assessment quickly identifies an optimal drone route. Therefore, four algorithms—i.e., Genetic Algorithm (GA) (Whitley 1994), Ant Colony Optimization (ACO) (Dorigo et al. 2006), Particle Swarm Optimization (PSO) (Poli et al. 2007), and BITmask Evolution OPTimization (BITEOPT) (Vaneev 2021)—are investigated in this study. Their performance is evaluated to provide benchmarks for future drone mission planning at disaster sites. These algorithms are briefly described in the following.

Genetic Algorithm. GA is a stochastic global search optimization method, inspired by natural selection theory. The algorithm transforms the process of solving a searching problem into a process similar to the crossover and mutation of chromosomes during biological evolution. It consists of five phases: initial population, fitness function, selection, crossover, and mutation. The algorithm first initializes a new population. Then, a fitness function is created, based on the total collected scores, to evaluate the solution. The selection phase selects the two pairs of best fit individuals in the population, based on the fitness score. The crossover operation is applied to those two pairs of individuals, with an exchange rate of 0.6. Finally, the output is fed into a mutation operator, in order to maintain the diversity of the population, by flipping bit at random positions with a probability of 0.005. A new offspring population is generated after mutation and crossover operations. The fitness, selection, crossover, and mutation processes repeat until the population does not change for 6,000 steps.

Ant Colony Optimization. The ACO algorithm is a metaheuristic method that was inspired by the foraging behavior of ants. The algorithm can be divided into three steps. First, algorithm parameters and "pheromone trails" are initialized. Second, each drone constructs a feasible route from initialized pheromone trails using the roulette method. Third, the quality of the route is evaluated based on the sum of surveyed damage indices. The second and third steps repeat 30 times; the route with the highest reward is selected.

Particle Swarm Optimization. PSO is a global optimization method inspired by the motion of flocks of birds. The algorithm consists of five steps. In the first step, the number of particles and iteration, the position of the particles, and the velocities of particles are initialized based on the number of drones and the number of damaged buildings. In the second step, the mutation operation is applied on the initialized particle swarm with a probability of 0.4. The proportion of particles is set to 0.5, and the mutation position of each particle is set to 0.5. In the third step, local optimization is conducted to separate small subsets of particle swarms, in order to avoid getting stuck on any local optimum. In the fourth step, the velocity of each particle position is updated based on both current and historical global optimal particle positions. The position of each particle is then updated based on its current position and the updated velocity. Finally, the total collected score is calculated, and the optimal solution is updated. The number of iterations is set to 4000.

BITmask Evolution OPTimization. BITEOPT is a stochastic non-linear bound-constrained derivative-free optimization algorithm for global optimization. This algorithm is a self-optimizing approach without any hyperparameters to fine-tune. In the beginning, the Gaussian sampling method is used to generate an initial solution. At the same time, several other populations are created in the proximity of the candidate solution. Depending on the quality of the candidate solution, a histogram formed by parameter values is updated. The histogram is used as a probability-state-automata to allow the algorithm to switch between algorithm flow paths. In addition, the route with the highest cost is replaced with the upper bound cost constraint. For each iteration, a new candidate solution generator is randomly selected from a list of solution generators. Note that the previous solution also serves as an independent parameter vector for the new solution generator. A total of 2,000,000 iterations are used to ensure an optimal drone mission plan.

EXPERIMENT AND RESULTS

Results on building damage recognition

Implementation details

The network is trained on a workstation running Windows 10 with an Intel Xeon Gold 5122 CPU, 64 GB of RAM, and an NVIDIA Quadro P5000 GPU. The Stochastic Gradient Descent (SGD) optimizer is used to train the network. The network is trained for a total of 300 epochs. The EFSBD dataset is randomly split into a training set (80%), a validation set (10%), and a testing set (10%). The images are resized to 640 x 640. The confidence and IoU thresholds for Non-maximum Suppression (NMS) operation are set to 0.1 and 0.4, respectively. The early stopping technique is used to avoid the overfitting problem. Specifically, the network stops training if the loss value does not decrease for 100 epochs. The model with the highest performance on the validation set is used for the evaluation on the testing set. The hyperparameters are given in Table 3.

Metrics

In this study, the average precision (AP) at the IoU threshold 0.5 (AP_{50}), and mean average precision (mAP) over different IoU thresholds, are used to quantify network performance. AP is the area under the precision-recall curve, defined in Eq. (18). The average of AP for all the classes is defined in Eq. (19) and expressed as AP, in order to differentiate it from mAP, where *nc* represents the number of classes. Since different IoU thresholds can produce different predictions, mAP was used to overcome this problem by averaging AP scores on different IoU thresholds. In this study, mAP is calculated as an average of AP over 10 IoUs, starting from 0.5 to 0.95 with a step size of 0.05, which has been used as a standard metric for evaluating object detection methods. Therefore, mAP is used as the metric to evaluate the overall performance of the model.

$$\mathrm{AP}' = \int_0^1 \mathrm{precision}(\mathrm{recall})\,d(\mathrm{recall}) \tag{18}$$

$$\mathrm{AP} = \frac{1}{nc}\sum_{i=1}^{nc} \mathrm{AP}_i' \tag{19}$$

Network performance

Table 4 presents the model performance on the testing dataset of the EFSBD dataset for each damage level. The network achieves an AP_{50} of 91.3% and an mAP score of 71.9% on the testing set of the EFSBD dataset. The results of the proposed method indicate a strong variation in performance across different levels of building damage. In particular, the proposed method results in the highest performance on the considerable damage category with an mAP of 80.9%, followed by an mAP of 80.8% on the moderate category. This may be attributed to a relatively large number of damaged building instances rated as moderate and considerable in the EFSBD dataset. The tarp category achieves an mAP of 78.2%. The relatively good performance for this category is due to the distinct features of buildings covered with roof tarps. The devastating damage category achieves the lowest performance with an mAP of 47.1%.

Fig. 7 presents the confusion matrix for the proposed method on the testing set of the EFSBD dataset. The matrix is normalized by the column, so that diagonal values represent recall for each category. Recall measures the predictive power of the network in identifying all the positive elements. The tarp category achieves the highest recall score on both validation and testing datasets. Specifically, the tarp category achieves a recall of 94% on the validation dataset and a recall of 96% on the testing dataset. The considerable damage category achieves the second-highest recall score, with a recall of 90% and 94% on the validation and testing dataset, respectively. A high recall score indicates that most positive samples for this category can be accurately detected. Note that the mAP score for the tarp is lower than those of the moderate and considerable categories, which could be attributed to a relatively smaller precision score for the tarp compared to those of the moderate and considerable categories. The incredible category has the lowest recall 76% on the validation set, and all the misclassified samples are background. Buildings rated as having incurred incredible damage each have the entire house swept away from its foundation, in which case there is no need for a detailed assessment. Therefore, misclassifying incredible damage as background will not have an impact on drone mission planning. For other levels of damages, misclassifying positive samples as background will lead to missing inspections during drone surveys. The confusion matrix also indicates that positive samples are mostly misclassified as adjacent categories, except for background. For instance, on the testing set, 4% and 1% of severely damaged buildings are misclassified as considerable and devastating, respectively. This is because the closer the damage levels are, the more similar the visual features are.

Fig. 8 illustrates example results of damage detection on the testing set of the EFSBD dataset. The results indicate that the proposed method can accurately recognize damaged buildings and their levels of damage.

Ablation study

In this section, an ablation study is conducted to assess the effectiveness of the two proposed improvements on the YOLOv5s network. The YOLOv5s is used as the baseline model. The effectiveness of alpha-IoU and coordinate attention are evaluated by individually integrating them into the baseline model. Table 5 presents the results on the testing set of the EFSBD dataset. The performance of the network is evaluated using mAP. The results indicate that the baseline network is mostly improved by alpha-IoU, with an improvement of 1.1%. The coordinate attention module improves on the performance of the baseline by 0.2%. A combination of alpha-IoU and coordinate attention achieves the best performance, which has an improvement of 1.4%. This improvement demonstrates the effectiveness of the proposed method in detecting and classifying building damage.

Model generalizability

While the proposed method achieves promising results on the EFSBD dataset, images in the training and testing sets could be extracted from the same disaster site. It is anticipated that, in real practice, the annotated dataset is not likely to be available for each new disaster site. In addition, the new video data could be captured from a different angle or altitude, in different weather conditions, and using a different camera. Therefore, the generalizability of the proposed method is further evaluated on completed unseen data. Specifically, four individual disaster sites are selected in the EFSBD dataset: Chattanooga, TN, Birmingham, AL, Springdale, AR, and Oak Grove, MO. For the evaluation on each of these disaster sites, images excluding those of the evaluated place are used as training data to train the network.

Table 6 shows the model performance on four unseen places. The results indicate significant performance variations across different sites. In particular, the model achieves the best performance in Birmingham, with an mAP of 47.7%. In Oak Grove, the proposed method achieves the worst performance, with an mAP of 23%. The results indicate that AP_{50} is greater than 40% in Chattanooga, Birmingham, and Springdale, which demonstrates the generalizability of the proposed method for unseen disaster sites.

Results on drone mission planning

To evaluate the performance of drone mission planning, a community in Chattanooga, TN, severely hit by an EF3 tornado in 2020 is selected. Fig. 9 shows the boundary of the study area. The square footage of the study area is approximately 670,000 m^2. The model, trained using images from other places, is used to predict building damages in the selected area. As mentioned above, the proposed method achieves an AP_{50} of 41% and an mAP of 25.9%, indicating its applicability in detecting and classifying building damage. In this study, the predicted building damage is used to update the digital building damage map. Note that, for some buildings, there may be two overlapped detections with different damage levels, which are typically adjacent levels of building damage. In this case, the level of damage with higher confidence is selected. Under current practices, the preliminary digital building damage map is generally created using satellite images (Khodaverdizahraee et al. 2020). However, satellite images have low resolution, and the viewing angle may not be favorable for building damage detection. Compared to satellite images, drone images have higher resolutions, and the oblique observations from a drone can provide more detailed façade and roof information. Therefore, the building damage detection results from drone images can be used to refine and update building damage maps.

The damage index refers to the DOD, as adopted by the tornado damage survey. The DODs for minor, moderate, considerable, severe, devastating, and incredible are 2, 4, 6, 8, 9, and 10, respectively, according to the damage survey conducted by the Center for Severe Weather Research (Marshall et al. 2008). While incredible damage has the highest DOD of 10, it indicates that anchored homes were swept away from their foundations; in such cases, assessing damages does not require high-resolution images or detailed information. Therefore, the buildings with incredible damages are excluded at the stage of drone mission planning. As for buildings with roofing tarp, they typically suffered from either minor or moderate damage, and the fine-grained level of damage is hard to recognize; thus, the DOD is set to 3. Fig. 10 shows the building damage map. Note that some damaged buildings are not indicated on the map. This is for two reasons. First, the proposed method fails to detect some damaged buildings, due to unfavorable angles.

Second, some of the damaged buildings are not visible from the collected video. In total, 193 damaged buildings are detected, with a total DOD of 727 in this region.

In this study, the time required to survey each of the damaged buildings is assumed to be dependent on DOD. This is reasonable, as tornado damage assessment typically focuses on the hardest-hit areas to estimate the EF scale. Therefore, buildings with higher levels of damage require a more detailed inspection to help surveyors in their assessments. In addition, in the case of high-level building damage suffered from severe structural damage, structural engineers need detailed information in order to determine the mechanism of building failure and to develop tornado-resistant building standards. Specifically, the survey time is set to 5 × DOD. Table 7 shows the experimental settings for drone mission planning. Three scenarios with different operational constraints are investigated. Specifically, the low scenario replicates the situation with very limited resources, and simulates two drones, each with a flight speed of 2.1 m/s and a battery life of 10 mins. The moderate scenario simulates three drones, each with a speed of 4.6 m/s and a battery life of 20 mins. The high scenario simulates four drones, each with a flying speed of 6.1 m/s and a battery life of 30 mins.

Fig. 11 shows a comparison of the GA, ACO, PSO, and BITEOPT algorithms in terms of total collected scores and processing speeds. Given the fact that these algorithms are stochastic-based methods, each of them is run 10 times for a fair comparison. The results indicate that the BITEOPT algorithm achieves the best performance under low and moderate scenarios, followed by the PSO algorithm. Under high scenarios, PSO and BITEOPT both visit all the damaged buildings. ACO has the worst performance among the four algorithms, though it has the fastest processing speed. While PSO achieves the second-best performance, its processing time is much higher than that of the other three algorithms. The processing speed of BITEOPT is the lowest, excluding ACO. It can be concluded that BITEOPT has the best performance among the investigated algorithms in solving multi-drone mission planning for building damage survey. Therefore, the authors recommend the use of BITEOPT in future drone mission planning for disaster reconnaissance. Fig. 12 shows sample optimization results for the GA, ACO, PSO, and BITEOPT algorithms.

DISCUSSION

Comparison with other state-of-the-art methods

This section compares the performance of the proposed method to other state-of-the-art methods. MSNet achieved an AP_{50} score of 31.5% on the ISBDA dataset in detecting bounding boxes of damaged buildings (Zhu et al. 2021). The total number of parameters were around 44 million. The training images were resized to have longer sides less than or equal to 1333. The proposed method was trained on the provided train-validation split. For a fair comparison, the input images are resized to 1280 x 1280. Using the provided train-validation split, the proposed method achieves significantly better performance, with an AP_{50} of 34.5%.

Pi et al. (2020) used YOLOv2 to identify ground objects of interests, such as damaged roofs, debris, and undamaged buildings, in the aftermath of a hurricane. The highest AP_{50} reported on unseen testing datasets were 24.5% for drone and 13.9% for helicopter. The inference speed of YOLOv2 is approximately 40 FPS. Cheng et al. (2021) developed a hybrid deep learning model in order to localize building objects and to classify the level of building damage. The model achieved an AP of 63.3% in building localization and an accuracy of 30% on building damage classification for drone data collected at a new location. Combined, the method's accuracy in detecting and classifying building damage from images was lower than 30%. Furthermore, the inference speed for the localization model was only 2.87 FPS and 20.12 FPS for the classification model. In comparison, our method achieved a minimum AP_{50} of 31.6% (at Oak Grove) and a maximum AP_{50} of 65.5% (at Birmingham). Furthermore, our proposed method only has 7.1 million parameters, achieving an inference speed of 70 FPS. The results indicate that our method outperforms other state-of-the-art approaches. It is acknowledged that the same set of data should be used to compare all these methods and to assess their performance under varying disaster scenarios. This requires access to these datasets and algorithms, which would call for further efforts pursuant to an evaluation benchmark.

Influence of image and network size

This section discusses the effect of image resolution and network size in the task of assessing building damages. Table 8 shows the performance of the proposed method over various image resolutions. The results indicate that the mAP score increases with increasing image resolutions. In particular, the network has the largest performance increase from 416 x 416 to 640 x 640, which carries an mAP improvement of 4.4%. The network performance improves by 2% when increasing image resolution from 640 x 640 to 1536 x 1536. From 832 x 832 to 1536 x 1536, the network only has a slight mAP improvement of 0.9%. On the other hand, the inference time of the network also increases with increasing image resolution. The inference speed is evaluated using the NVIDIA Quadro P5000 GPU. The inference speed of 416 x 416 reaches 87 FPS. When image resolution is increased to 640 x 640, the inference FPS drops to 70. The selection of image resolution is a trade-off between accuracy and speed. In this study, 640 x 640 is chosen for fast building damage detection with due accuracy.

Table 9 presents a comparison of the proposed method with other networks in the family of YOLOv5 with larger network sizes. The results indicate that model performance increases with the increasing size of the network from YOLOv5s to YOLOv5x. YOLOv5x exhibits an mAP improvement of 3.7%, compared to YOLOv5s. The proposed method outperforms YOLOv5m with a much smaller network. The small network has the potential to be integrated into an embedded system for building damage detection. While larger-sized networks tend to perform better, they require more storage and come with increased computation costs, which work against their deployment in mobile platforms such as drones.

Sensitivity of drone mission planning

The performance of drone mission planning is affected by operational constraints. In this section, the BITEOPT algorithm is selected for the sensitivity analysis, since it achieved the best performance under the low, moderate, and high scenarios. The sensitivity of the number of drones, flight speed, and battery life is analyzed. The number of drones ranges from two to five. The flight speeds of the drones are 2.1, 4.6, and 6.1 m/s. The battery lives are 10, 20, and 30 mins. The results reported are averaged over 10 runs. Fig. 13 (a) presents the sensitivity of the number of drones. The drone speed is fixed at 4.6 m/s and the battery life is fixed at 20 mins. The results show an increasing trend in total collected scores with increases in the number of drones.

Fig. 13 (b) shows the sensitivity of the flight speed of the drone. The number of drones is fixed at three, and the battery life is fixed at 20 mins. The results indicate that the greater the flight speed is, the higher the collected scores are. Fig. 13 (c) displays the score variation over battery life of the drone. In the experiment, the number of drones is fixed at three, and the flight speed is fixed at 4.6 m/s. The results indicate that the collected score is significantly improved by increased battery life. In summary, the performance of the BITEOPT algorithm is positively related to the availability of resources.

Limitations and future research directions

Future research is needed in several directions. First, in this study, the building damage map was manually created based on network prediction results from aerial images. The proposed network is very lightweight, which affords it the potential to be integrated into a drone's onboard platform for online building damage detection. Under current practices, tornado damage surveyors upload damage information to an online database through the NOAA damage assessment toolkit, which is time-consuming and labor-intensive. Future research could develop methods for automatically uploading detected damaged buildings to NOAA online database according to the GPS coordinates of the buildings. In this way, survey teams can not only have timely disaster damage information, but also building damage maps to assess overall damage, which in turn would facilitate better disaster responses.

Second, while our method achieves state-of-the-art performance on unseen data, there is a lot of room for further improvement. The improvement will mainly come from two research directions. One is the building damage data; the other is the building damage detection method. For data-driven methods, a large dataset is always the foundation for ensuring performance and generalizability in real-world applications. In this direction, the developed EFSBD dataset needs to be updated through the collection of more data, especially images from distinctive locations, so as to increase the model's generalizability. On the other hand, with the advancement of deep learning architectures, the detection network can also be upgraded by integrating new architectures for more robust performance.

Third, this study is limited to demonstrating the feasibility and superiority of damage-aware drone mission planning. Though the optimization algorithm is demonstrated to be suitable and effective in identifying routes for multi-drone missing planning, how such a method can improve or complement existing tornado damage surveys remains unexplored. In addition, this study assumes that the required survey time for buildings with different levels of damage accords with tornado damage assessment in actual practice. Finally, the rationale behind building damage detection and classification using the deep learning network remains unexplored in this study. Ideally, the deep learning network needs to follow a rationale similar to that of field assessors for building damage assessment. The development of such an approach requires close collaboration with field assessment teams, so as to better understand their rationales for building damage assessment at disaster sites. In the future, this research team will test the feasibility and applicability of its approach by collaborating with survey teams from the NWS and Tennessee Emergency Management Agency. The feedback from these professional organizations is critical to improving our methods, validating field performance, and developing off-the-shelf products that are ready for use.

CONCLUSIONS

This study develops a new method for automated building damage reconnaissance and drone mission planning for disaster response. The practical utility of the proposed methods is sustained by two computational innovations as well as the high performance validated using real-world data and scenarios. Most existing deep-learning-based methods only detect and classify damaged buildings and non-damaged buildings and provide limited information to first responders and decision-makers. The developed method is superior to existing solutions, as it can accurately detect and classify seven categories of damages consistently at a high frame rate. This is achieved by preparing an unprecedented dataset to achieve robust performance, as well as incorporating a new attention mechanism in the deep learning method for detection and classification. This automated building damage reconnaissance method achieved an AP_{50} of 91.3% and an mAP of 71.9% on the testing dataset, and the model was applied to a new location with very promising results; three of four selected disaster areas achieved an AP_{50} higher than 40%. The proposed method is very lightweight and achieves fast detection with an FPS of 70. Thus, the AI method can be developed in an embedded system for building damage detection while the drone is on a mission. The building damage information acquired from drones is computationally modeled in the drone mission planning optimization model, and different solution methods are utilized to identify the best suitable method. The BITEOPT optimization method exhibits the best performance and can identify optimal routes for multiple drones. The computational time is less than six minutes for an area of 193 damaged buildings, further demonstrating this model's practical utility for real disaster mission planning optimization. The methods and workflow are validated using a case study of a tornado disaster, demonstrating that automating the retrieval of building damage information can significantly augment drone-based mission planning during disaster response and mitigation.

DATA AVAILABILITY STATEMENTS

All data, models, or codes that support the findings of this study are provided by the corresponding author upon reasonable request.

ACKNOWLEDGEMENTS

This research was funded by the U.S. National Science Foundation (NSF) via Grants 1850008 and 2129003, Tennessee Department of Transportation (TDOT) via the contract RES2021-05 "Drones and Other Technologies to Assist Disaster Relief Efforts", and Science Alliance at the University of Tennessee Knoxville. The authors gratefully acknowledge the support from NSF, TDOT, and Science Alliance. Any opinions, findings, recommendations, and conclusions in this paper are those of the authors, and do not necessarily reflect the views of NSF, TDOT, The University of Tennessee, Knoxville, The University of Florida, and The University of Texas at San Antonio.

REFERENCES

Baker, J. W., and C. A. Cornell. 2008. "Uncertainty propagation in probabilistic seismic loss estimation." *Structural Safety*, 30 (3): 236–252. Elsevier. https://doi.org/10.1016/j.strusafe.2006.11.003.

Buratti, N., F. Minghini, E. Ongaretto, M. Savoia, and N. Tullini. 2017. "Empirical seismic fragility for the precast RC industrial buildings damaged by the 2012 Emilia (Italy) earthquakes." *Earthquake Engineering & Structural Dynamics*, 46 (14): 2317–2335. Wiley Online Library. https://doi.org/10.1002/eqe.2906.

Chang, L., A. S. Elnashai, and B. F. Spencer Jr. 2012. "Post-earthquake modelling of transportation networks." *Structure and infrastructure Engineering*, 8 (10): 893–911. Taylor & Francis.

Chao, I.-M., B. L. Golden, and E. A. Wasil. 1996. "The team orienteering problem." *Eur J Oper Res*, 88 (3): 464–474. Elsevier. https://doi.org/10.1016/0377-2217(94)00289-4.

Chen, J., S. Li, D. Liu, and X. Li. 2020. "AiRobSim: Simulating a Multisensor Aerial Robot for Urban Search and Rescue Operation and Training." *Sensors*, 20 (18): 5223. MDPI AG. https://doi.org/10.3390/s20185223.

Chen, J., S. Li, D. Liu, and W. Lu. 2022. "Indoor camera pose estimation via style-transfer 3D models." *Computer-Aided Civil and Infrastructure Engineering*, 37 (3): 335–353. https://doi.org/10.1111/mice.12714.

Chen, J., W. Lu, and F. Xue. 2021. "'Looking beneath the surface': A visual-physical feature hybrid approach for unattended gauging of construction waste composition." *Journal of Environmental Management*, 286: 112233. Elsevier. https://doi.org/10.1016/j.jenvman.2021.112233.

Chen, L., H. Zhang, J. Xiao, L. Nie, J. Shao, W. Liu, and T.-S. Chua. 2017. "Sca-cnn: Spatial and channel-wise attention in convolutional networks for image captioning." *Proceedings of the IEEE conference on computer vision and pattern recognition*, 5659–5667.

Chen, S.-C., M. Chen, N. Zhao, S. Hamid, K. Chatterjee, and M. Armella. 2009. "Florida public hurricane loss model: Research in multi-disciplinary system integration assisting government policy making." *Government Information Quarterly*, 26 (2): 285–294. Elsevier. https://doi.org/10.1016/j.giq.2008.12.004.

Cheng, C., A. H. Behzadan, and A. Noshadravan. 2021. "Deep learning for post-hurricane aerial damage assessment of buildings." *Computer-Aided Civil and Infrastructure Engineering*, 36 (6): 695–710. Wiley Online Library. https://doi.org/10.1111/mice.12658.

Cooner, A. J., Y. Shao, and J. B. Campbell. 2016. "Detection of urban damage using remote sensing and machine learning algorithms: Revisiting the 2010 Haiti earthquake." *Remote Sensing*, 8 (10): 868. Multidisciplinary Digital Publishing Institute. https://doi.org/10.3390/rs8100868.

Cornell, C. A., F. Jalayer, R. O. Hamburger, and D. A. Foutch. 2002. "Probabilistic basis for 2000 SAC federal emergency management agency steel moment frame guidelines." *Journal of structural engineering*, 128 (4): 526–533. American Society of Civil Engineers. https://doi.org/10.1061/(ASCE)0733-9445(2002)128:4(526).

Dorigo, M., M. Birattari, and T. Stutzle. 2006. "Ant colony optimization." *IEEE Comput Intell Mag*, 1 (4): 28–39. IEEE. https://doi.org/10.1109/MCI.2006.329691.

Doswell, C. A., H. E. Brooks, and N. Dotzek. 2009. "On the implementation of the enhanced Fujita scale in the USA." *Atmospheric Research*, 93 (1–3): 554–563. Elsevier. https://doi.org/10.1016/j.atmosres.2008.11.003.

Doyle Rice. 2022. "Weather disasters broke records and killed over 600 Americans in 2021." Accessed January 29, 2022. https://www.usatoday.com/story/news/nation/2022/01/10/weather-2021-death-toll/9157670002/.

Du, A., J. Cai, and S. Li. 2021. “Metamodel-based state-dependent fragility modeling for Markovian sequential seismic damage assessment.” *Engineering Structures*, 243: 112644. Elsevier. https://doi.org/10.1016/j.engstruct.2021.112644.

Du, A., and J. E. Padgett. 2020. “Investigation of multivariate seismic surrogate demand modeling for multi-response structural systems.” *Engineering Structures*, 207: 110210. Elsevier. https://doi.org/10.1016/j.engstruct.2020.110210.

Du, A., and J. E. Padgett. 2021. “Entropy-based intensity measure selection for site-specific probabilistic seismic risk assessment.” *Earthquake Engineering & Structural Dynamics*, 50 (2): 560–579. Wiley Online Library. https://doi.org/10.1002/eqe.3346.

Du, A., J. E. Padgett, and A. Shafieezadeh. 2020. “Influence of intensity measure selection on simulation-based regional seismic risk assessment.” *Earthquake Spectra*, 36 (2): 647–672. SAGE Publications Sage UK: London, England. https://doi.org/10.1177/8755293019891717.

FEMA. 2012. *Hazus-MH 2.1–Earthquake model technical manual*. Washington, D.C.

Geiß, C., H. Taubenböck, S. Tyagunov, A. Tisch, J. Post, and T. Lakes. 2014. “Assessment of seismic building vulnerability from space.” *Earthquake Spectra*, 30 (4): 1553–1583. SAGE Publications Sage UK: London, England.

Giordano, N., F. de Luca, A. Sextos, F. Ramirez Cortes, C. Fonseca Ferreira, and J. Wu. 2021. “Empirical seismic fragility models for Nepalese school buildings.” *Natural Hazards*, 105 (1): 339–362. Springer. https://doi.org/10.1007/s11069-020-04312-1.

Gramajo, G., and P. Shankar. 2017. “An Efficient Energy Constraint Based UAV Path Planning for Search and Coverage.” *International Journal of Aerospace Engineering*, 2017. Hindawi Limited. https://doi.org/10.1155/2017/8085623.

Grogan, S., R. Pellerin, and M. Gamache. 2021. “Using tornado-related weather data to route unmanned aerial vehicles to locate damage and victims.” *OR Spectrum*, 43 (4): 905–939. Springer Science and Business Media Deutschland GmbH. https://doi.org/10.1007/S00291-021-00640-1/TABLES/13.

Guo, M.-H., T.-X. Xu, J.-J. Liu, Z.-N. Liu, P.-T. Jiang, T.-J. Mu, S.-H. Zhang, R. R. Martin, M.-M. Cheng, and S.-M. Hu. 2022. “Attention mechanisms in computer vision: A survey.” *Computational Visual Media*, 1–38. Springer. https://doi.org/10.1007/s41095-022-0271-y.

Gupta, R., B. Goodman, N. Patel, R. Hosfelt, S. Sajeev, E. Heim, J. Doshi, K. Lucas, H. Choset, and M. Gaston. 2019. “Creating xBD: A dataset for assessing building damage from satellite imagery.” *Proceedings of the IEEE/CVF conference on computer vision and pattern recognition workshops*, 10–17.

Hayat, S., E. Yanmaz, C. Bettstetter, and T. X. Brown. 2020. “Multi-objective drone path planning for search and rescue with quality-of-service requirements.” *Autonomous Robots*, 44 (7): 1183–1198. Springer. https://doi.org/10.1007/S10514-020-09926-9/FIGURES/10.

He, J., S. Erfani, X. Ma, J. Bailey, Y. Chi, and X.-S. Hua. 2021. “$\alpha $-IoU: A Family of Power Intersection over Union Losses for Bounding Box Regression.” *Advances in Neural Information Processing Systems*, 34.

Herbin, A. H., and M. Barbato. 2012. “Fragility curves for building envelope components subject to windborne debris impact.” *Journal of Wind Engineering and Industrial Aerodynamics*, 107: 285–298. Elsevier. https://doi.org/10.1016/j.jweia.2012.05.005.

Hou, Q., D. Zhou, and J. Feng. 2021. “Coordinate attention for efficient mobile network design.” *Proceedings of the IEEE/CVF Conference on Computer Vision and Pattern Recognition*, 13713–13722.

Hu, D., J. Chen, and S. Li. 2022a. “Reconstructing unseen spaces in collapsed structures for search and rescue via deep learning based radargram inversion.” *Automation in Construction*, 140: 104380. Elsevier. https://doi.org/10.1016/j.autcon.2022.104380.

Hu, D., J. Chen, S. Li, and V. R. Kamat. 2019. “Detecting, Locating, and Characterizing Voids in Disaster Rubbles for Search and Rescue.” *Advanced Engineering Informatics*, Under revi: 100974. https://doi.org/10.1016/j.aei.2019.100974.

Hu, D., L. Chen, J. Du, J. Cai, and S. Li. 2022b. “Seeing through Disaster Rubble in 3D with Ground-Penetrating Radar and Interactive Augmented Reality for Urban Search and Rescue.” *Journal of Computing in Civil Engineering*, 36 (5): 04022021. American Society of Civil Engineers. https://doi.org/10.1061/(ASCE)CP.1943-5487.0001038.

Hu, D., and S. Li. 2022. “Recognizing object surface materials to adapt robotic disinfection in infrastructure facilities.” *Computer-Aided Civil and Infrastructure Engineering*. Wiley Online Library. https://doi.org/10.1111/mice.12811.

Hu, D., H. Zhong, S. Li, J. Tan, and Q. He. 2020. “Segmenting areas of potential contamination for adaptive robotic disinfection in built environments.” *Building and Environment*, 184: 107226. Elsevier Ltd. https://doi.org/10.1016/j.buildenv.2020.107226.

Hu, J., L. Shen, S. Albanie, G. Sun, and E. Wu. 2017. “Squeeze-and-Excitation Networks.” *IEEE Transactions on Pattern Analysis and Machine Intelligence*, 42 (8): 2011–2023. IEEE Computer Society.

Huang, Z., C. Chen, and M. Pan. 2020. “Multiobjective UAV Path Planning for Emergency Information Collection and Transmission.” *IEEE Internet of Things Journal*, 7 (8): 6993–7009. Institute of Electrical and Electronics Engineers Inc. https://doi.org/10.1109/JIOT.2020.2979521.

Van Huynh, D., T. Do-Duy, L. D. Nguyen, M. T. Le, N. S. Vo, and T. Q. Duong. 2022. “Real-Time Optimized Path Planning and Energy Consumption for Data Collection in Unmanned Ariel Vehicles-Aided Intelligent Wireless Sensing.” *IEEE Transactions on Industrial Informatics*, 18 (4): 2753–2761. IEEE Computer Society. https://doi.org/10.1109/TII.2021.3114358.

Jocher, G., A. Stoken, A. Chaurasia, N. Jirka Borovec, TaoXie, Y. Kwon, K. Michael, C. Liu, J. Fang, A. V, L. Tkianai, YxNONG, P. Skalski, A. Hogan, J. Nadar, and L. M. Imyhxy. 2021. “ultralytics/yolov5: v6.0 - YOLOv5n ‘Nano’ models, Roboflow integration, TensorFlow export, OpenCV DNN support (v6.0).” *Zenodo*. Accessed May 18, 2022. https://zenodo.org/record/5563715#.Yobjxy-B27g.

Kakooei, M., and Y. Baleghi. 2017. “Fusion of satellite, aircraft, and UAV data for automatic disaster damage assessment.” *International Journal of Remote Sensing*, 38 (8–10): 2511–2534. Taylor and Francis Ltd. https://doi.org/10.1080/01431161.2017.1294780.

Khodaverdizahraee, N., H. Rastiveis, and A. Jouybari. 2020. “Segment-by-segment comparison technique for earthquake-induced building damage map generation using satellite imagery.” *International journal of disaster risk reduction*, 46: 101505. Elsevier. https://doi.org/10.1016/j.ijdrr.2020.101505.

Lei, L. P., L. Y. Liu, L. Zhang, J. T. Bi, Y. H. Wu, Q. Jiao, and W. Zhang. 2010. “Assessment and analysis of collapsing houses by aerial images in the Wenchuan earthquake.” *J. Remote Sens*, 14 (2): 333–344.

Li, B., S. Patankar, B. Moridian, and N. Mahmoudian. 2018. “Planning Large-Scale Search and Rescue using Team of UAVs and Charging Stations∗.” *2018 IEEE International Symposium on Safety, Security, and Rescue Robotics, SSRR 2018*. Institute of Electrical and Electronics Engineers Inc. https://doi.org/10.1109/SSRR.2018.8468631.

Liu, S., L. Qi, H. Qin, J. Shi, and J. Jia. 2018. “Path aggregation network for instance segmentation.” *Proceedings of the IEEE conference on computer vision and pattern recognition*, 8759–8768.

Marshall, T. P., D. McCarthy, J. G. LaDue, J. Wurman, C. R. Alexander, P. Robinson, and K. Kosiba. 2008. “Damage survey and deduction of vortex structure of the Greensburg, KS tornado.” *24th Conf. Severe Local Storms*.

McDonald, J. R., K. C. Mehta, D. A. Smith, and J. A. Womble. 2009. “The Enhanced Fujita Scale: Development and Implementation.” *Forensic Engineering 2009*, 719–728. Reston, VA: American Society of Civil Engineers.

Miura, H., T. Aridome, and M. Matsuoka. 2020. “Deep learning-based identification of collapsed, non-collapsed and blue tarp-covered buildings from post-disaster aerial images.” *Remote Sensing*, 12 (12). https://doi.org/10.3390/rs12121924.

Murphy, R. R., E. Steimle, C. Griffin, C. Cullins, M. Hall, and K. Pratt. 2008. “Cooperative use of unmanned sea surface and micro aerial vehicles at Hurricane Wilma.” *Journal of Field Robotics*, 25 (3): 164–180. John Wiley & Sons, Ltd. https://doi.org/10.1002/rob.20235.

Nedjati, A., G. Izbirak, B. Vizvari, and J. Arkat. 2016. “Complete coverage path planning for a multi-UAV response system in post-earthquake assessment.” *Robotics*, 5 (4): 26. Multidisciplinary Digital Publishing Institute.

Nielson, B. G., and R. DesRoches. 2007. “Seismic fragility methodology for highway bridges using a component level approach.” *Earthq Eng Struct Dyn*, 36 (6): 823–839. Wiley Online Library. https://doi.org/10.1002/eqe.655.

Padgett, J. E., and R. DesRoches. 2008. “Methodology for the development of analytical fragility curves for retrofitted bridges.” *Earthquake Engineering & Structural Dynamics*, 37 (8): 1157–1174. Wiley Online Library. https://doi.org/10.1002/eqe.801.

Pi, Y., N. D. Nath, and A. H. Behzadan. 2020. “Convolutional neural networks for object detection in aerial imagery for disaster response and recovery.” *Advanced Engineering Informatics*, 43: 101009. Elsevier. https://doi.org/10.1016/j.aei.2019.101009.

Pinelli, J.-P., G. Pita, K. Gurley, B. Torkian, S. Hamid, and C. Subramanian. 2011. “Damage characterization: Application to Florida public hurricane loss model.” *Natural Hazards Review*, 12 (4): 190–195. American Society of Civil Engineers. https://doi.org/10.1061/(ASCE)NH.1527-6996.0000051.

Poli, R., J. Kennedy, and T. Blackwell. 2007. “Particle swarm optimization.” *Swarm intelligence*, 1 (1): 33–57. Springer. https://doi.org/10.1007/s11721-007-0002-0.

Qi, J., D. Song, H. Shang, N. Wang, C. Hua, C. Wu, X. Qi, and J. Han. 2016. “Search and Rescue Rotary-Wing UAV and Its Application to the Lushan Ms 7.0 Earthquake.” *Journal of Field Robotics*, 33 (3): 290–321. John Wiley & Sons, Ltd. https://doi.org/10.1002/rob.21615.

Rahnemoonfar, M., T. Chowdhury, A. Sarkar, D. Varshney, M. Yari, and R. R. Murphy. 2021. “Floodnet: A high resolution aerial imagery dataset for post flood scene understanding.” *IEEE Access*, 9: 89644–89654. IEEE. https://doi.org/10.1109/ACCESS.2021.3090981.

Redmon, J., S. Divvala, R. Girshick, and A. Farhadi. 2016. “You only look once: Unified, real-time object detection.” *Proceedings of the IEEE conference on computer vision and pattern recognition*, 779–788.

Roueche, D. B., F. T. Lombardo, and D. O. Prevatt. 2017. “Empirical approach to evaluating the tornado fragility of residential structures.” *Journal of Structural Engineering*, 143 (9): 04017123. American Society of Civil Engineers. https://doi.org/10.1061/(ASCE)ST.1943-541X.0001854.

Schaefer, M., R. Teeuw, S. Day, D. Zekkos, P. Weber, T. Meredith, and C. J. van Westen. 2020. "Low-cost UAV surveys of hurricane damage in Dominica: automated processing with co-registration of pre-hurricane imagery for change analysis." *Natural Hazards*, 101 (3): 755–784. Springer.

Vaneev, A. 2021. "BITEOPT - Derivative-Free Optimization Method." Accessed May 18, 2022. https://github.com/avaneev/biteopt.

Vickery, P. J., F. J. Masters, M. D. Powell, and D. Wadhera. 2009. "Hurricane hazard modeling: The past, present, and future." *Journal of Wind Engineering and Industrial Aerodynamics*, 97 (7–8): 392–405. Elsevier. https://doi.org/10.1016/j.jweia.2009.05.005.

Wang, C.-Y., H.-Y. M. Liao, Y.-H. Wu, P.-Y. Chen, J.-W. Hsieh, and I.-H. Yeh. 2020. "CSPNet: A new backbone that can enhance learning capability of CNN." *Proceedings of the IEEE/CVF conference on computer vision and pattern recognition workshops*, 390–391.

Whitley, D. 1994. "A genetic algorithm tutorial." *Statistics and Computing*, 4 (2): 65–85. Springer. https://doi.org/10.1007/BF00175354.

Xie, S., J. Duan, S. Liu, Q. Dai, W. Liu, Y. Ma, R. Guo, and C. Ma. 2016. "Crowdsourcing rapid assessment of collapsed buildings early after the earthquake based on aerial remote sensing image: A case study of Yushu earthquake." *Remote Sensing*, 8 (9): 759. Multidisciplinary Digital Publishing Institute. https://doi.org/10.3390/rs8090759.

Xu, F., Y. Zhang, R. Wang, C. Mi, Y. Zhang, Y. Huang, and J. Yang. 2021. "Heuristic Path Planning Method for Multistatic UAV-Borne SAR Imaging System." *IEEE Journal of Selected Topics in Applied Earth Observations and Remote Sensing*, 14: 8522–8536. Institute of Electrical and Electronics Engineers Inc. https://doi.org/10.1109/JSTARS.2021.3106449.

Yamazaki, F., Y. Yano, and M. Matsuoka. 2005. "Visual damage interpretation of buildings in Bam city using QuickBird images following the 2003 Bam, Iran, earthquake." *Earthquake Spectra*, 21 (SUPPL. 1). SAGE PublicationsSage UK: London, England. https://doi.org/10.1193/1.2101807.

Yu, X., C. Li, and J. F. Zhou. 2020. "A constrained differential evolution algorithm to solve UAV path planning in disaster scenarios." *Knowledge-Based Systems*, 204: 106209. Elsevier. https://doi.org/10.1016/J.KNOSYS.2020.106209.

Zhang, R., H. Li, K. Duan, S. You, K. Liu, F. Wang, and Y. Hu. 2020. "Automatic detection of earthquake-damaged buildings by integrating UAV oblique photography and infrared thermal imaging." *Remote Sensing*, 12 (16): 2621. Multidisciplinary Digital Publishing Institute. https://doi.org/10.3390/RS12162621.

Zhu, X., J. Liang, and A. Hauptmann. 2021. "MSNet: A Multilevel Instance Segmentation Network for Natural Disaster Damage Assessment in Aerial Videos." *2021 IEEE Winter Conference on Applications of Computer Vision (WACV)*, 2022–2031. IEEE.

Table 1 Description of Enhanced Fujita Scale building damage indicators

Level	***Damage indicator***
Minor	Some damage to roof covering and/or lost some of their vinyl or metal siding.
Moderate	Lost most of roof covering and/or had minor structural damage to roof such as displaced gable ends and/or loss of some roof decking.
Considerable	Most of roof structure was lost but the walls remain standing.
Severe	Roofs and numerous outside walls blown away from frame homes; two-story homes have their second floor destroyed; high-rises have many windows blown out.
Devastating	All walls went down, and a pile of debris remained on their foundation.
Incredible	Anchored homes were swept away from their foundation.
Tarp	Roof covered with a roofing tarp.

Table 2 Overview of existing natural disaster aerial datasets

Dataset	Disaster	Size	Building instances	Image type	Task	Category
AIDER (Kyrkou and Theocharides 2020)	Fire, flood, collapsed building, …	2,545	-	Drone	Classification	5
Volan2018 (Pi et al. 2020)	Hurricane	65,580	98,010	Drone	Object detection	6
ISBDA (Zhu et al. 2021)	Hurricane, tornado	1,030	2,961	Aerial	Semantic segmentation	3
FloodNet (Rahnemoonfar et al. 2021)	Hurricane	2,343	6,675	Drone	Semantic segmentation	8
RescueNet (Chowdhury et al. 2022)	Hurricane	4,494	10,903	Drone	Semantic segmentation	11
EFSBD (ours)	Tornado	3,045	24,496	Drone	Object detection	7

Table 3 Hyperparameters for model training

Parameter	Value	Parameter	Value
Initial learning rate	0.01	IoU training threshold	0.2
Learning rate factor	0.01	Anchor-multiple threshold	4
Momentum	0.937	HSV-hue augmentation	0.015
Weight decay	0.005	HSV-saturation augmentation	0.4
Warmup epochs	3	HSV-value augmentation	0.4
Warmup momentum	0.8	Rotation	0.2
Warmup learning rate	0.1	Translation	0.1
Box loss gain	0.05	Scale	0.5
Classification loss gain	0.5	Flip up-down	0.2
Classification BCELoss positive weight	1	Flip left-right	0.5
Object loss gain	1	Mosaic	1
Object BCELoss positive weight	1	Segment copy-paste	0.2

Table 4 Model performance on the testing set of EFSBD dataset

Class	Labels	AP_{50} (%)	mAP (%)
All	2542	91.3	71.9
Minor	486	90.1	75.6
Moderate	757	94.8	80.8
Considerable	594	96.2	80.9
Severe	275	92.1	71.9
Devastating	90	82.2	47.1
Incredible	45	88.5	69.0
Tarp	295	95.3	78.2

Table 5 Ablation study of the proposed method on the testing set of EFSBD dataset

Model	mAP (%)
YOLOv5s	70.5
YOLOv5s + alpha-IoU	71.6
YOLOv5s + coordinate attention	70.7
YOLOv5s + alpha-IoU + coordinate attention (**Proposed**)	**71.9**

Table 6 Model performance on unseen disaster sites

Place	Images	AP_{50} (%)	mAP (%)
Chattanooga, TN	369	41.0	25.9
Birmingham, AL	145	65.5	47.7
Springdale, AR	87	40.4	29.9
Oak Grove, MO	67	31.6	23.0

Table 7 Experiment settings of drone mission planning

Scenario	Number of UAV	Speed of UAV (m/s)	Battery life (mins)
Low	2	2.1	10
Moderate	3	4.6	20
High	4	6.1	30

Table 8 Effect of image resolution on network performance

Resolution	AP_{50} (%)	mAP (%)	Time (ms)
416 x 416	89.0	67.5	11.4
640 x 640	91.3	71.9	13.7
832 x 832	91.5	73.0	18.9
1280 x 1280	91.3	73.4	36.4
1536 x 1536	91.7	73.9	49.6

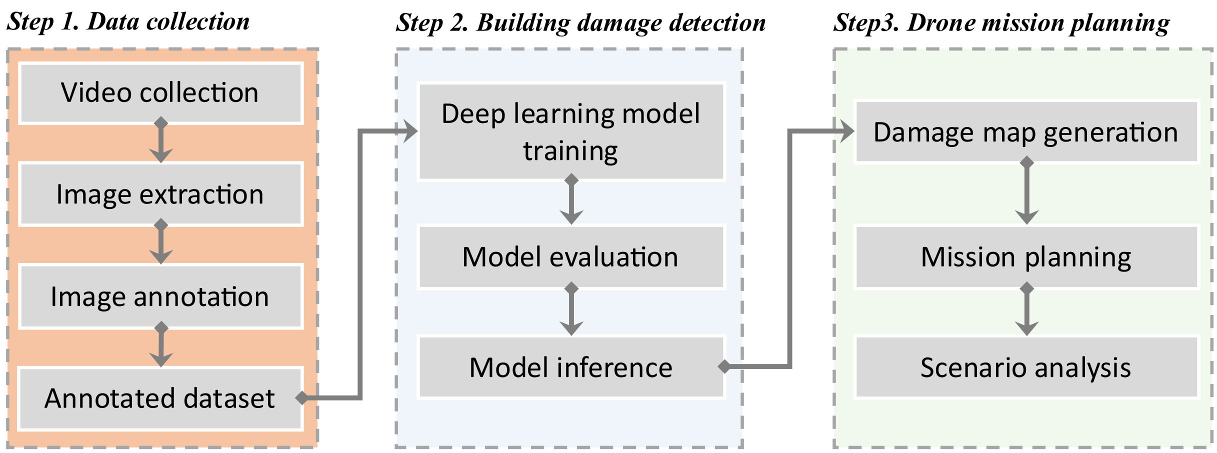

Fig. 1. Methodology overview

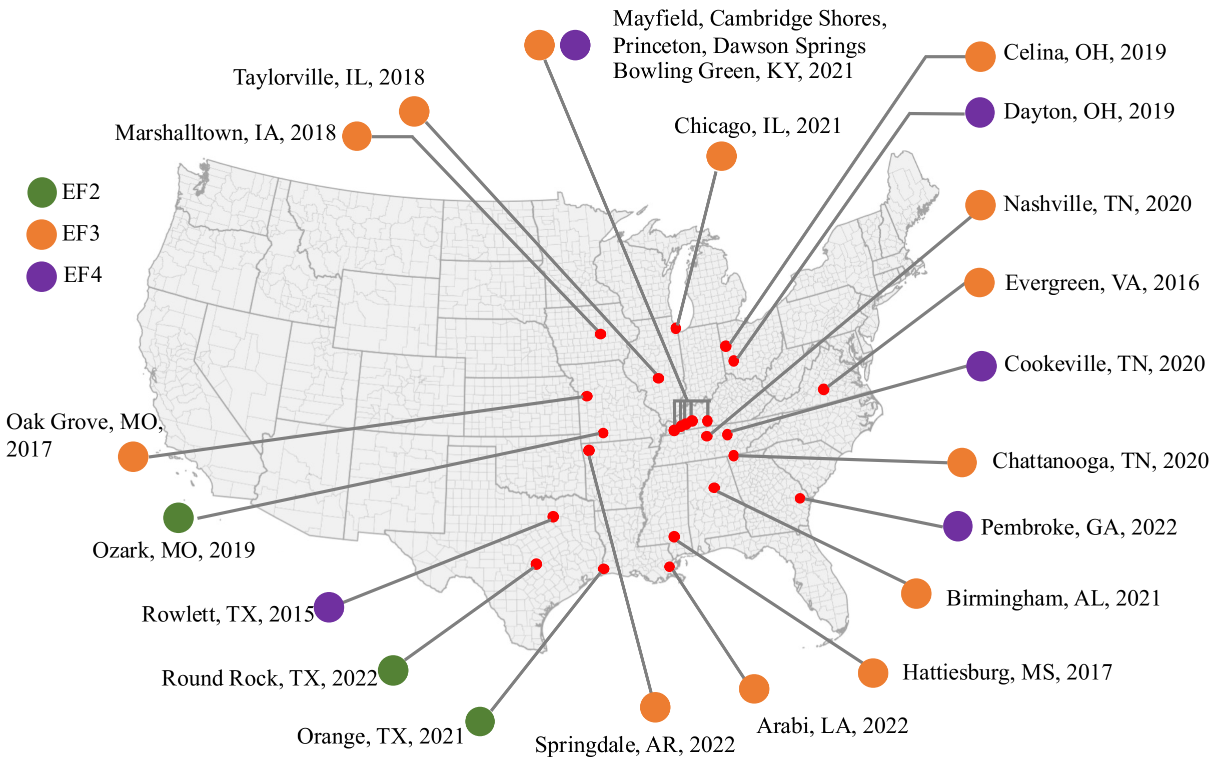

Fig. 2 EF scale and approximate locations of selected U.S. tornados represented in the dataset

Minor | Moderate | Considerable | Severe

Devastating | Incredible | Tarp

Fig. 3 Example of damaged buildings with different levels (Images by National Weather Service and National Oceanic and Atmospheric Administration)

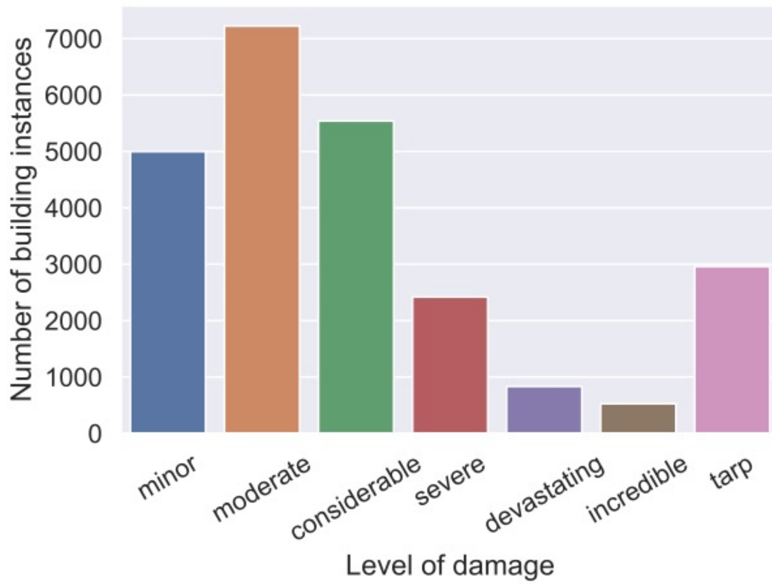

Fig. 4 EFSBD dataset statistics

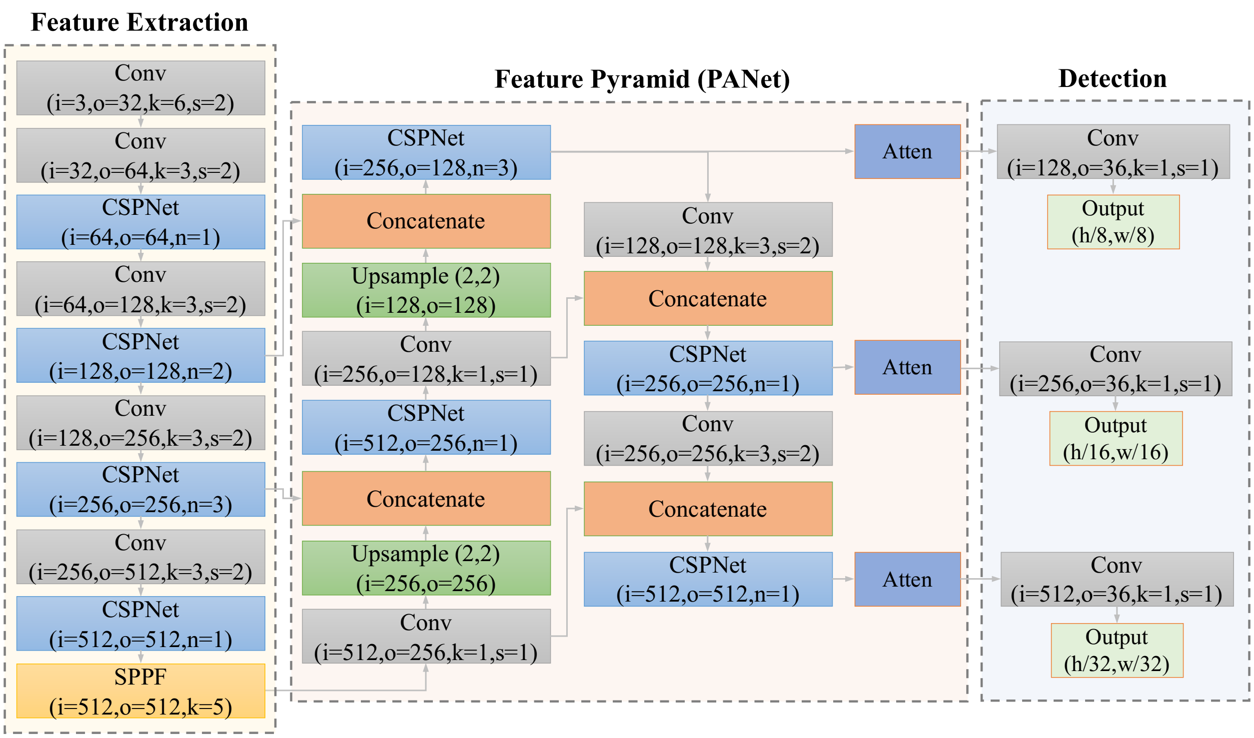

Fig. 5 Architecture of the proposed network

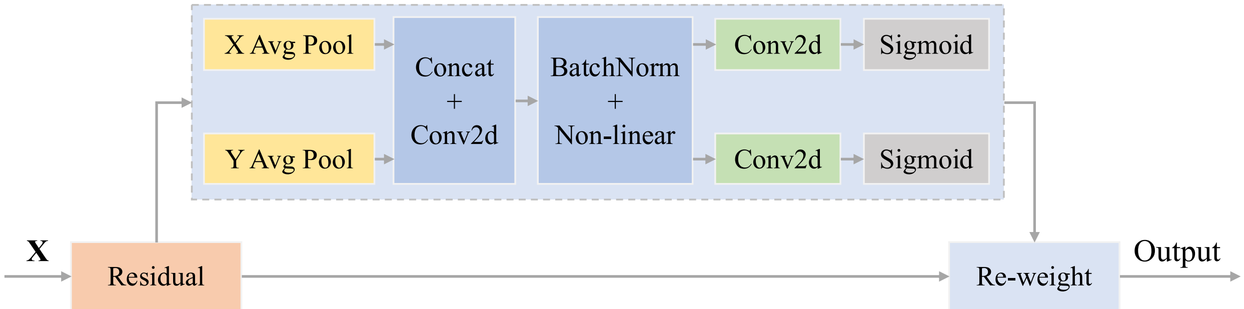

Fig. 6 Flowchart of coordinate attention mechanism

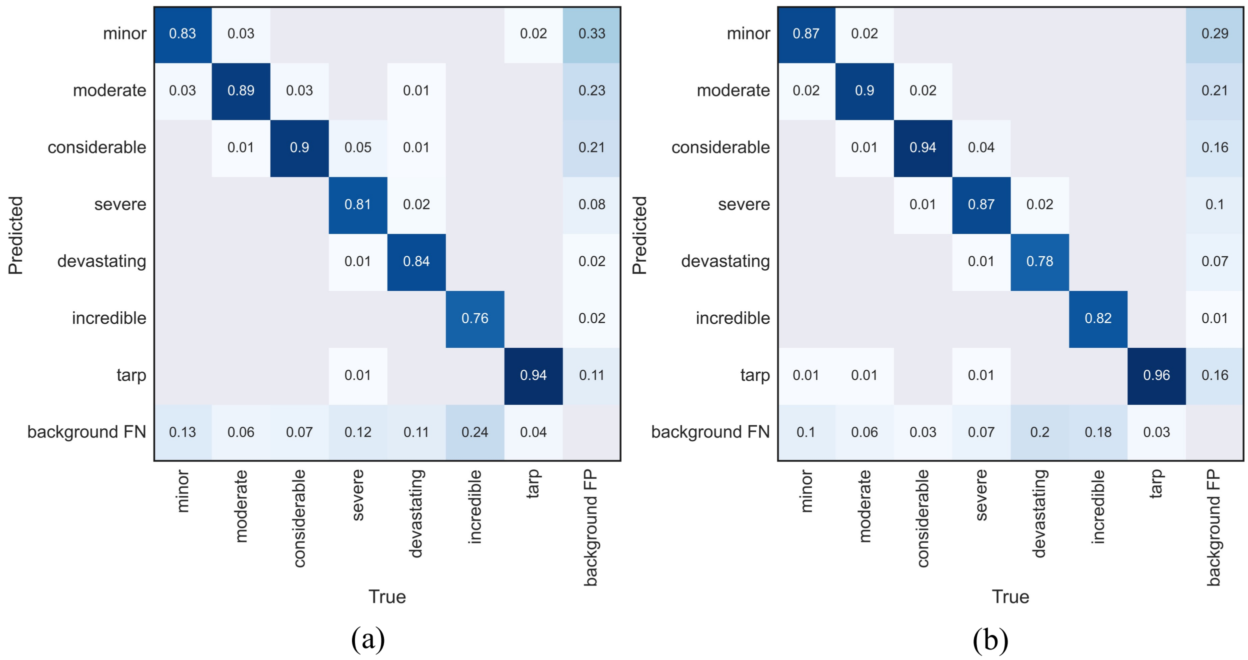

Fig. 7 Confusion matrix for the proposed method on the validation and testing datasets of EFSBD dataset.

(a) validation dataset; and (b) testing dataset

Fig. 8 Examples of detection results on the testing set of EFSBD dataset (Images by authors)

Fig. 9 Study area in Chattanooga, TN, USA. (map data: Google, Maxar technologies)

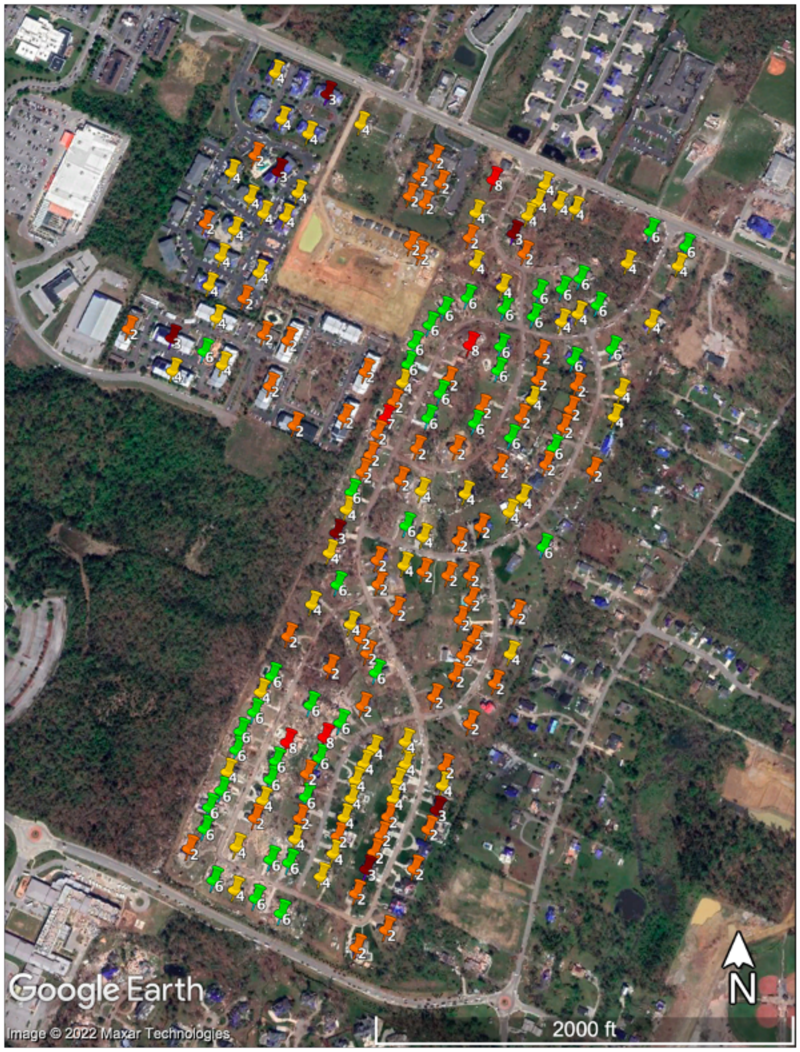

Fig. 10 Building damage map. Note: Each marker represents a damaged building; different color represents different levels of damage (map data: Google, Maxar technologies)

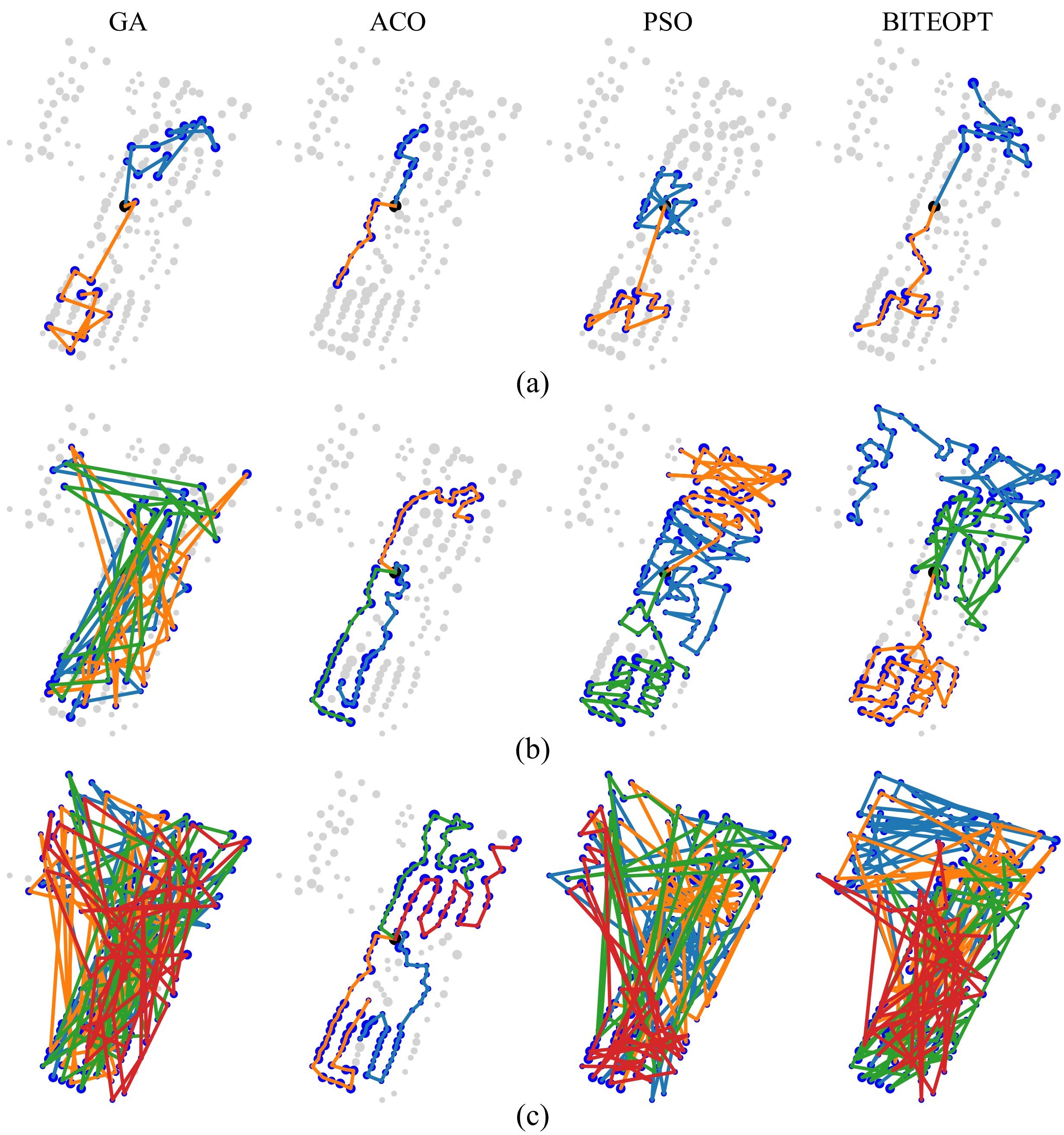

Fig. 11 Performance comparison of drone mission planning algorithms. (a) total collected score; and (b) processing speed

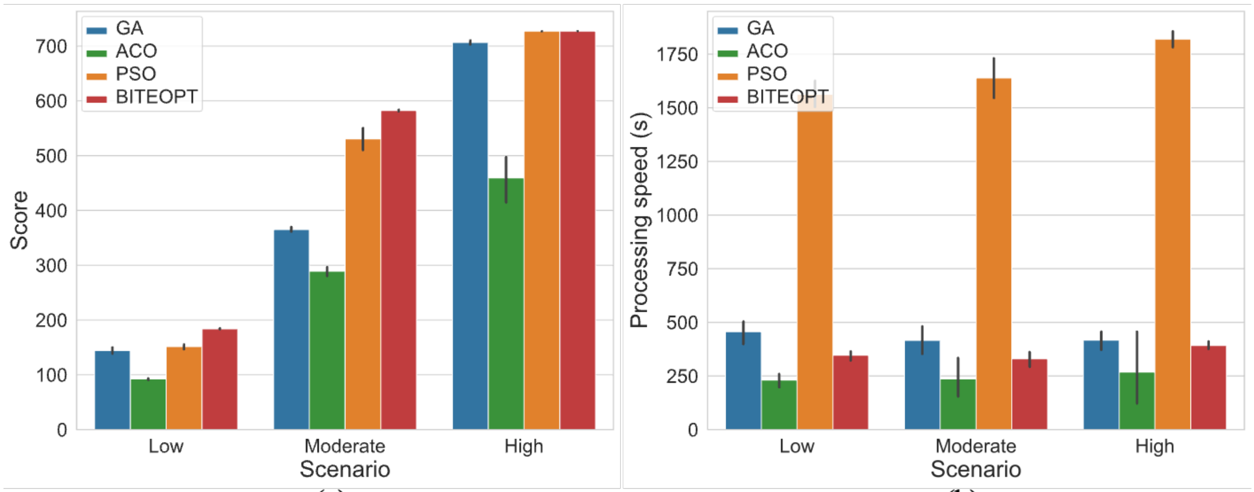

(a) (b)

Fig. 12 Example optimization results of GA, ACO, PSO, and BITEOPT under low, moderate, and high scenarios. (a) low; (b) moderate; and (c) high. Note: gray circle represents unvisited buildings; blue circle represents visited buildings; black circle represents the starting point; the size of the circle represents the degree of damage; the edge connects two buildings represents the route of the drone; and the color of the edge represents the routes for different drones

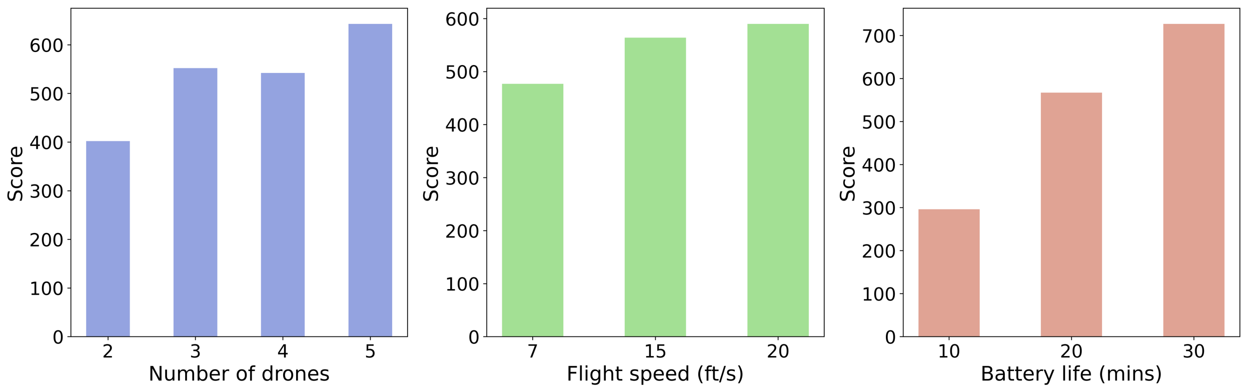

(a) (b) (c)

Fig. 13 Sensitivity analysis of BITEOPT algorithm. (a) number of drones; (b) flight speed; and (c) battery life